IET Renewable Power Generation

Research Article

ZSI for PV systems with LVRT capability

ISSN 1752-1416
Received on 16th January 2018
Accepted on 14th May 2018
doi: 10.1049/iet-rpg.2018.5104
www.ietdl.org

Sally Sajadian[1], *Reza Ahmadi*[1] ✉

[1]*Department of Electrical Engineering and Computer Science, University of Kansas, KS, USA*

✉ *E-mail: ahmadi@ku.edu*

Abstract: This study proposes a power electronics interface (PEI) for photovoltaic (PV) applications with a wide range of ancillary services. As the penetration of distributed generation systems is booming, the PEI for renewable energy sources should be capable of providing ancillary services such as reactive power compensation and low-voltage ride through (LVRT). This study proposes a robust model predictive-based control strategy for grid-tied *Z*-source inverters (ZSIs) for PV applications with LVRT capability. The proposed system has two operation modes: normal grid condition and grid fault condition modes. In normal grid condition mode, the maximum available power from the PV panels is injected into the grid. In this mode, the system can provide reactive power compensation as a power conditioning unit for ancillary services from DG systems to main ac grid. In case of grid faults, the proposed system changes the behaviour of reactive power injection into the grid for LVRT operation according to the grid requirements. Thus, the proposed controller for ZSI is taking into account both the power quality issues and reactive power injection under abnormal grid conditions. The proposed system operation is verified experimentally, the results demonstrate fast dynamic response, small tracking error in steady-state, and simple control scheme.

1 Introduction

Power systems are commonly made up of large central power plants that feed power to the transmission and distribution systems to supply the loads. However, due to the recent increasing interest in exploiting renewable energy resources, the distributed generation (DG) facilities that are interfaced directly to the distribution network (DN) are becoming ubiquitous. Photovoltaic (PV) generation systems are one of the most widely adopted DG facilities that are frequently connected to DN. The existing DN was not initially built with a concern for high-level DG integration, thus the recent trend is leading to degraded DN system performance, safety, and reliability. Some of the well known concerns pertaining to the integration of more DG into the DN are the power quality issues, frequency stability, islanding operation mode, voltage stability, protection issues, and increased fault currents [1–6]. Therefore, several grid codes and standards have been issued to regulate DG systems integration with the DN [7–10].

The future PV connected to DN should be able to provide a wide range of ancillary services due to grid mandates and codes [11]. Thus, the PV inverters should be able to operate in different modes of operations under grid faults such as intentional islanding [12, 13] and low-voltage ride through (LVRT) mode with reactive power compensation capability [14–16]. In addition to these ancillary services, highly reliable and efficient power electronics interface (PEI) for PV systems are required to harvest maximum available power from PV panels. PV systems commonly use two-stage power conversion [17, 18]: an upstream dc/dc power conversion stage from the PV module to a dc-link energy buffer (such as a capacitor), and a downstream dc/ac power conversion stage from the energy buffer to the grid. The use of a two-stage PEI is required due to the inherent limitation of the conventional dc/ac inverters for regulating the voltage freely. This two-stage power conversion decreases the efficiency of the system and limits the dynamic response of the system in harsh PV ambient condition and grid perturbation. Therefore, an efficient and reliable PEI for PV sources in DG systems requires a single-stage power conversion with robust control strategy considering the grid status to meet the grid codes and standards.

A few research works have been recently published focusing on the LVRT operation for two-stage and single-stage grid-tied PV systems using classical multi-loop controllers [14, 15, 19]. As mentioned earlier, the two-stage power conversion suffers from low efficiency and limited dynamic response [20, 21]. The single-stage power conversion also suffers from an inability to freely step down/up the voltage, because they are either voltage-source or current-source inverters [20, 22]. In addition, LVRT operation appears to be challenging since many additional cascaded loops are required for traditional control scheme of PV systems [15, 19]. In addition, the use of multi-loop controller causes slow dynamic response under harsh PV ambient condition or/and abnormal grid condition.

Impedance-source inverters are able to overcome several limitations of voltage-source and current-source inverters [20, 22]. In particular, the *Z*-source inverter (ZSI) can step up/down the voltage freely [20]; therefore, they are a well-suited single-stage PEI for PV sources in DG systems [23–25]. However, the ZSIs' operation and modulation are different than conventional inverters due to the existence of impedance network at their input port. Also, the required LVRT operation will add additional control complexity in comparison with conventional control strategies for ZSIs. In [23], a unified control scheme for grid-tied ZSI for PV applications is proposed with reactive power compensation. The presented method uses a modified space vector pulse-width modulation (SVPWM) to achieve a shoot-through mode. This requires complex modulation scheme with multi–nested-loop control strategy. A control scheme of ZSI for PV application with integrated energy storage is proposed in [24], the proposed control scheme does not consider ancillary services for grid-tied operation. A grid-tied PV system based on series ZSI is proposed in [21]; the control objectives are the maximum power point tracking (MPPT) and grid current. An indirect dc-link control is proposed to achieve constant peak dc-link voltage. An SVPWM modulation scheme is used. The grid current is regulated at unity power factor.

Model predictive control (MPC) [26] is a suitable solution for ZSIs with different modes of operations and multi-objective control functionality. Comparing to classical control schemes, MPC techniques deliver fast dynamic response with high stability marking, making them well suited for PV systems [27] in harsh ambient condition and abnormal grid condition. Also, for the ZSIs, the MPC eliminates the complex modulation stage required to implement the shoot-through state [28].

Unlike the previous works, this paper proposes a single-stage smart PV system for grid interaction based on ZSI and MPC framework with the capability to operate in LVRT mode. The main features of the proposed smart PEI are:

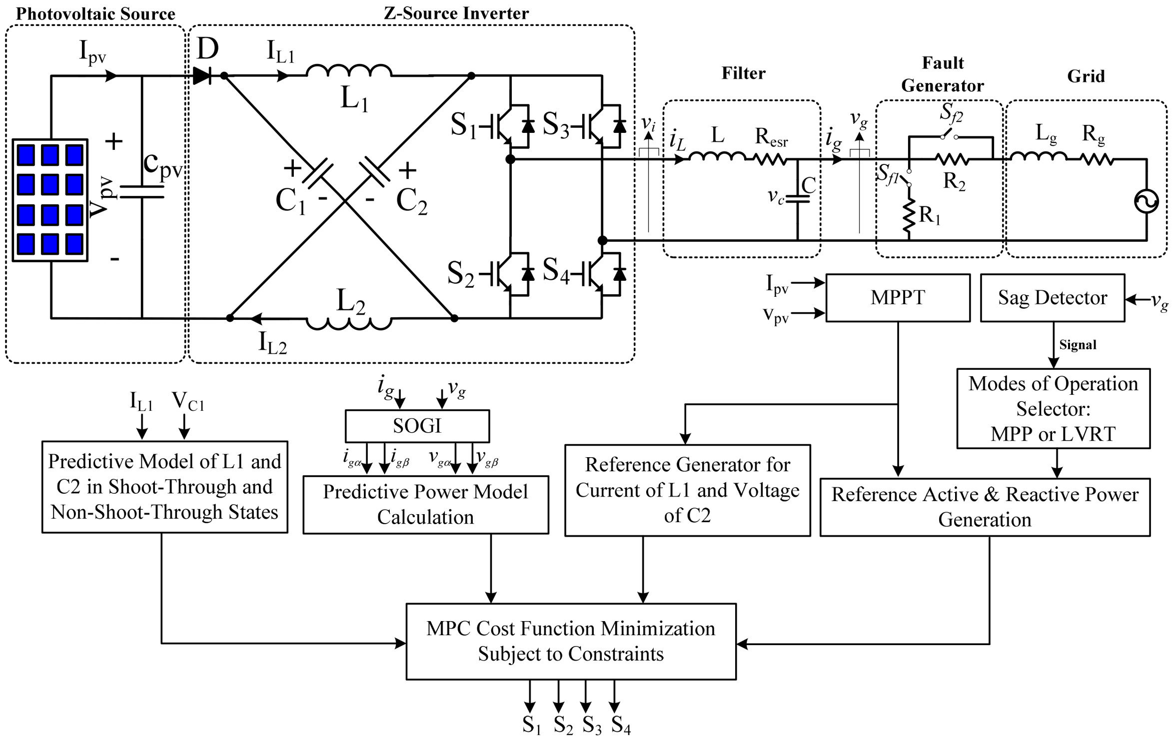

Fig. 1 *General schematic representation of the proposed PEI based on the ZSI for grid-tied PV application with LVRT capability*

(a) High efficiency and reliable operation due to a single power conversion stage.
(b) MPP operation under normal grid condition.
(c) Reactive power compensation.
(d) LVRT operation under grid faults such as voltage sag with reactive power compensation capability to meet the grid codes and standards.
(e) Simple control architecture without the requirement of many cascaded loops as in classical linear control methods for ZSIs.
(f) Fast dynamic response under harsh PV ambient condition and grid abnormalities.
(g) Negligible tracking error of controller objectives in steady-state PV ambient condition and normal grid condition.
(h) Seamless transition between MPPT and LVRT modes of operations.

2 Proposed predictive model control

2.1 System modelling

Fig. 1 illustrates the proposed smart PV system by model predictive-based control of ZSI with LVRT capability. This section presents the predictive modelling of the PV side impedance network and the grid-side filter. The dynamic model of the grid-side filter is given by

$$\frac{\mathrm{d}}{\mathrm{d}t}i_{\mathrm{L}}(t) = \frac{1}{L}(v_{\mathrm{i}}(t) - v_{\mathrm{g}}(t) - i_{\mathrm{L}}(t)R_{\mathrm{esr}}) \tag{1}$$

$$\frac{\mathrm{d}}{\mathrm{d}t}v_{\mathrm{C}}(t) = \frac{\mathrm{d}}{\mathrm{d}t}v_{\mathrm{g}}(t) = \frac{1}{C}(i_{\mathrm{L}}(t) - i_{\mathrm{g}}(t)) \tag{2}$$

where $i_{\mathrm{L}}(t)$ is the inductor current, $v_{\mathrm{i}}(t)$ is the output voltage of the inverter, $v_{\mathrm{g}}(t)$ is the ac grid voltage, L and C are the filter's inductance and capacitance values, and R_{esr} is the equivalent series resistance of the inductor. By applying the Euler forward approximation method to (1) and (2), the discretised models of (1) and (2) are found as

$$\tilde{i}_{\mathrm{L}}(k+1) = \frac{T_{\mathrm{s}}}{L}(v_{\mathrm{i}}(k) - v_{\mathrm{g}}(k) - i_{\mathrm{L}}(k)R_{\mathrm{esr}}) + i_{\mathrm{L}}(k) \tag{3}$$

$$\tilde{v}_{\mathrm{C}}(k+1) = \frac{T_{\mathrm{s}}}{C}(i_{\mathrm{L}}(k) - i_{\mathrm{g}}(k)) + v_{\mathrm{C}}(k) \tag{4}$$

where T_{s} is the sampling period.

One of the main characteristics of ZSI is its shoot-through mode for flexible boosting of the input (PV) voltage. In this mode, both switches in one leg of the inverter are simultaneously turned ON. The equivalent circuit model of the ZSI in Fig. 1 for shoot-through mode and non-shoot-through modes (active states) are illustrated in Figs. 2*a* and *b*. Using these equivalent circuits and Euler forward approximation, the predictive model of the *Z*-source network can be developed [29]. According to Abu-Rub *et al.* [29], the predictive equations for the inductor L_1 current and capacitor C_1 voltage in a non-shoot-through mode are

$$\tilde{I}_{\mathrm{L1}}(k+1) = I_{\mathrm{L1}}(k) + \frac{T_{\mathrm{S}}}{L_1}(V_{\mathrm{pv}}(k) - V_{\mathrm{C1}}(k) - R_{\mathrm{L1}}I_{\mathrm{L1}}(k)) \tag{5}$$

$$\tilde{V}_{\mathrm{C1}}(k+1) = V_{\mathrm{C1}}(k) + \frac{T_{\mathrm{S}}}{C_1}(I_{\mathrm{L1}}(k) - I_{\mathrm{inv}}(k)) \tag{6}$$

while the same equations for a shoot-through state are

$$\tilde{I}_{\mathrm{L1}}(k+1) = I_{\mathrm{L1}}(k) + \frac{T_{\mathrm{S}}}{L_1}(V_{\mathrm{C1}}(k) - R_{\mathrm{L1}}I_{\mathrm{L1}}(k)) \tag{7}$$

$$\tilde{V}_{\mathrm{C1}}(k+1) = V_{\mathrm{C1}}(k) - \frac{T_{\mathrm{S}}}{C_1}I_{\mathrm{L1}}(k) \tag{8}$$

The second-order general integrator (SOGI) [30] is used to determine the in-phase and quadrature component ($\alpha\beta$) of grid voltage and current. The characteristic transfer functions of SOGI in *S*-domain are given by [30]

$$\frac{x_{\alpha}(s)}{x(s)} = \frac{\chi\omega s}{s^2 + \chi\omega s + \omega^2} \tag{9}$$

$$\frac{x_{\beta}(s)}{x(s)} = \frac{\chi\omega^2}{s^2 + \chi\omega s + \omega^2} \tag{10}$$

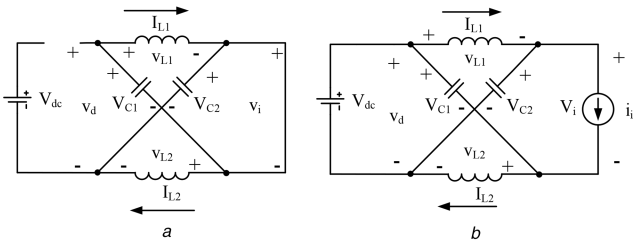

Fig. 2 *Equivalent circuit model of the impedance network of ZSI in Fig. 1 during shoot-through and non-shoot-through modes*
(a) Equivalent circuit in shoot-through mode, ***(b)*** Equivalent circuit in the non-shoot-through mode

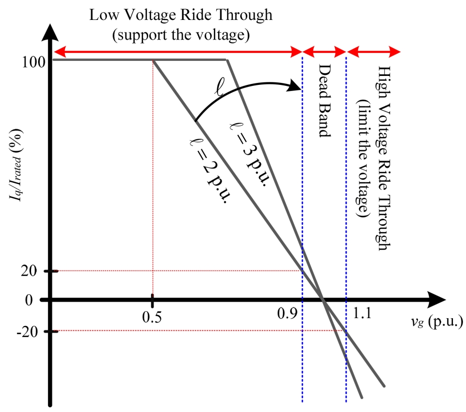

Fig. 3 *Grid-code requirement for reactive current injection, standard E.ON [14, 32–34]*

where χ is the damping factor and ω is the fundamental frequency. The SOGI can filter the harmonics that are far from the fundamental frequency. The SOGI can effectively extract the fundamental component from signals associated with harmonic components. Thus, using SOGI as the grid voltage $v_g(t)$ and grid current $i_g(t)$ can be formulated as

$$\begin{aligned} v_{g\alpha}(t) &= V_g \sin(\omega t) \\ i_{g\alpha}(t) &= I_g \sin(\omega t + \varphi) \end{aligned} \tag{11}$$

$$\begin{aligned} v_{g\beta}(t) &= V_g \sin(\omega t + \pi/2) \\ i_{g\beta}(t) &= I_g \sin(\omega t + \varphi + \pi/2) \end{aligned} \tag{12}$$

Using this terminology and the instantaneous power analysis [31], the predictive equations for the active and reactive powers can be determined as

$$\begin{aligned} \tilde{P}(k+1) &= P(k) - \omega T_s Q(k) \\ &\quad + \frac{T_s}{2L}\left(V_g^2 - v_{g\alpha}(k) v_{i\alpha}(k) - v_{g\beta}(k) v_{i\beta}(k)\right) \end{aligned} \tag{13}$$

$$\begin{aligned} \tilde{Q}(k+1) &= Q(k) + \omega T_s P(k) \\ &\quad - \frac{T_s}{2L}\left(v_{g\beta}(k) v_{i\alpha}(k) - v_{g\alpha}(k) v_{i\beta}(k)\right) \end{aligned} \tag{14}$$

2.2 Modes of operations

Next generation PEIs similar to the one shown in Fig. 1 for grid-connected PV systems needs to take into consideration the effects of reactive power injection into the grid under grid fault conditions. This is required according to grid standards and codes in addition to concern for the injected power quality.

The proposed system in Fig. 1 has two modes of operations: the MPP mode and the LVRT mode. In the MPP mode, the system operates at unity power factor and the maximum available active power from the PV is injected into the grid. The proposed system is also capable of providing reactive power for the grid as an ancillary service in the MPP mode. The system operates in MPP mode until the sag detector unit detects a grid voltage fault. After the fault detection, the controller triggers the mode change and the system enters the LVRT mode. In this mode, the system can tolerate the voltage drops for a short period of time. Simultaneously, the system injects reactive power into the grid to aid with re-establishing the grid voltage. The required reactive power injection in LVRT mode according to E.ON code [32] as an example is illustrated in Fig. 3. As pictured, the required reactive power to recover the voltage is a function of the grid voltage (v_g). In addition to the grid voltage stabilisation, in the LVRT mode, the avoidance of PV power generation can be realised [35]. The power generation profile during LVRT mode will be discussed in the next section.

2.3 Power profiles

The overcurrent protection strategy and required amount of reactive power by the grid in LVRT mode determine the reactive power injection strategy. The literature suggests several reactive power injection strategies for single-phase inverters [14, 33, 36]. Some notable examples are the constant active current strategy, the constant average active power strategy, and the constant peak current strategy [33, 36]. The constant active current strategy extracts the maximum available power from the PV array. In this method, the amplitude of the injected current to the grid may exceed the inverter maximum allowable current. This operation situation may lead to the failure of the whole system and thus increase the operation and maintenance costs. Another approach to maximise the power harvest from the PV array is to maintain the average injected active power at a constant value in the LVRT mode. This method is called constant average active power strategy. In this strategy also, there is a risk of overcurrent failure due to the demand for reactive power injection by the grid. In both aforementioned strategies, some constraints can be added to the controller to avoid inverter shutdown due to overcurrent protection. However, considering an existing inverter with a specific robustness margin, enforcing additional constraints limits the reactive power injection capability. Thus, in this situation, the active power generated by PV should be reduced to provide sufficient room for reactive power injection.

In this paper, constant peak current strategy is used as the power profile during the LVRT mode. In this method, the amplitude of the injected current to the grid is kept constant, thus the issue of overcurrent protection and inverter shutdown in the previous two aforementioned methods are avoided. The current (I_q) injected can be calculated according to Fig. 3 as

$$\begin{aligned} I_q &= \ell(1 - v_g) I_{\text{rated}} \\ &\quad \text{where}: 0.5\,\text{pu} \le v_g \le 0.9\,\text{pu} \\ \ell &\ge 2\,\text{pu} \end{aligned} \tag{15}$$

As it is shown in Fig. 3, for a specific grid voltage (v_g) and gain (ℓ), a certain level of reactive power should be injected into the grid according to the level of voltage sag. For example, for a 0.7 pu grid voltage (v_g) and $\ell = 2\,\text{pu}$, at least 70% of the rated grid current (I_{rated}) should be injected into the grid. If the grid voltage (v_g) is <0.5 pu, the ZSI will generate full reactive power ($I_q = I_{\text{rated}}$).

According to this grid code, the voltage control can have a dead band of ±0.1 as shown in Fig. 3. In this method, the maximum grid current is set as the rated current of the ZSI ($I_{g-\max} = I_{\text{rated}}$). The phasor diagram of the system under normal grid condition and during LVRT mode based on constant peak current strategy are illustrated in Fig. 4. As pictured, the injected active power to the grid is decreased in the LVRT mode.

2.4 Active and reactive power reference generations

Active and reactive power controls at the same time requires control of both of the power or their power components, i.e. i_d and i_q. In this paper, based on the mode of operation (MPPT or LVRT),

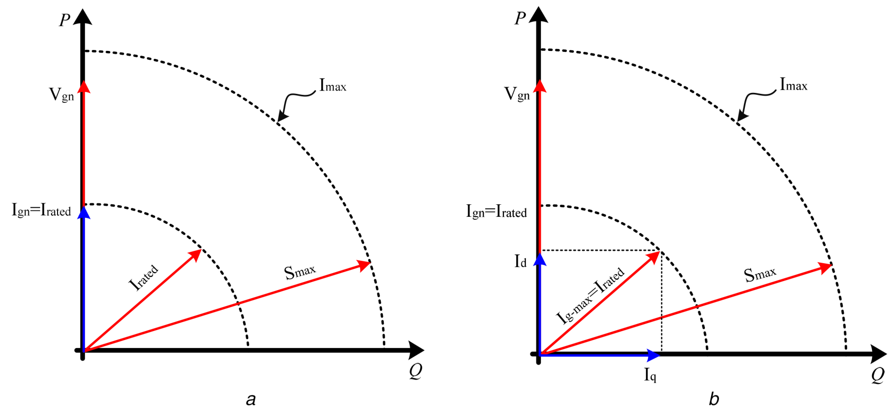

Fig. 4 *Power profile for single-phase grid-tied ZSI*
(a) Unity power factor power profile under normal grid condition, ***(b)*** Constant peak current power profile during LVRT operation

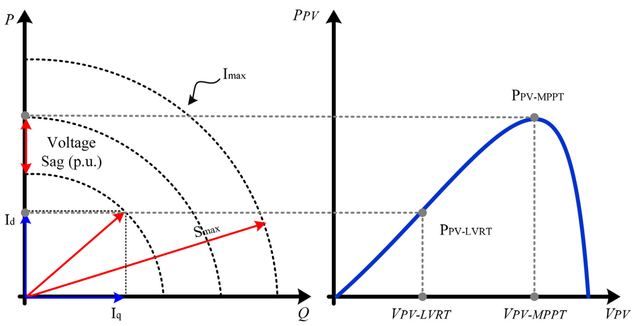

Fig. 5 *Power profile for single-phase grid-tied ZSI for PV application and P–V characteristics of PV panel when grid voltage sag occurs: the active power drawn from PV panel diminishes in the LVRT mode by moving from MPP operation coordinates when grid voltage sag occurs*

the power components are adjusted through controls of P and Q by MPC cost function. This section presents the active and reactive power reference generations for MPC cost function. During the normal grid condition operation, the reference for active power (P_{ref}) is determined by the MPPT unit. The previously developed model predictive-based MPPT in [37] is used to harvest the maximum available power from the PV array under normal grid condition. This model predictive-based MPPT method shifts the PV voltage to MPP voltage by adaptively incrementing/decrementing the future PV voltage according to proximity to MPP. The determined V_{PV} and I_{PV} can be used to calculate the P_{ref} in this mode of operation. This strategy minimises the oscillation around the MPP and improves the dynamic performance [37]. The reactive power reference (Q_{ref}) is set to zero for unity power factor operation in this mode of operation.

In the LVRT mode, the power reference is generated based on the grid requirement as shown in Fig. 3. Accordingly, the corresponding power factor in the LVRT mode can be expressed as

$$\cos\varphi = \begin{cases} \sqrt{1-\ell^2(1-v_g)^2}, & (1-1/\ell) < v_g < 0.9\,\text{pu} \\ 0, & v_g < (1-1/\ell)\text{pu} \end{cases} \tag{16}$$

As mentioned in the previous section, the peak of injected current from ZSI into the grid is kept at its rated current ($I_{\text{g-max}} = I_{\text{rated}}$), then current ($I_d$) in dq rotating reference frame can be calculated as

$$I_d = I_{\text{rated}}\sqrt{1-\ell^2(1-v_g)^2} \tag{17}$$

The required reactive current for injection can be determined by (15) in conjunction with grid-code standard E.ON which is illustrated in Fig. 3. This standard demonstrates the required reactive power by the grid based on the level of grid voltage sag. Thus, the reference active (I_d) and reactive current (I_q) in LVRT can be calculated according to the grid standard (Fig. 3) and (15) and (17) in the dq frame. Using the instantaneous power theory and calculated I_{dq}, the reference active (P_{ref}) and reactive (Q_{ref}) powers can be calculated.

Fig. 5 illustrates the graphical representation of the power drawn from PV array during MPPT and LVRT modes of operations. The constant peak current strategy limits the active current drawn from the PV panels in LVRT in order to prevent ZSI shutdown due to current protection. As shown in Fig. 5, depending on the depth of voltage sag according to Fig. 3, the injected active current to the grid is decreased to maintain the constant grid peak current when delivering the required reactive current to the grid according to grid standards (Fig. 3). Thus, the active powers drawn from the PV panels are decreased. In this situation, the PV power (P_{PV}) can be decreased by moving to the right or left of the MPP operating point. The proposed controller reduces the P_{PV} in the LVRT mode by shifting the operating point to the left of the MPP as shown in Fig. 5, because operation on the right-hand side of MPP may cause instability [38]. It is worth mentioning that this strategy for the proposed PEI can be used for the overnight operation of the PV system with energy storage in the absence of solar irradiance to support reactive power injection to the grid as an ancillary service.

2.5 MPC cost function minimisation

As mentioned in the previous section, the proposed system has two modes of operations: MPPT under normal grid condition and LVRT in case of grid voltage sag. Thus, a hybrid cost function for MPC needs to be developed. The control variables' references for the hybrid cost function is determined according to system's mode of operation, MPPT unit power output, and LVRT reference generation unit outputs. The sag detector triggers use of the appropriate weights in the hybrid cost function to change the mode from MPPT to LVRT. The designed cost function J is

$$\begin{aligned} &\min\ J^{\sigma\in[1,5]} = \sum_{n=1}^{2}\left(\lambda'_n g_P^\sigma + \lambda''_n g_Q^\sigma + \delta'_n g_{\text{L1}}^\sigma + \delta''_n g_{\text{C1}}^\sigma\right) \\ &\text{subject to } g_P^\sigma = \left|\tilde{P}^\sigma(k+1) - P_{\text{ref}}^n(k)\right|, \\ &\quad g_Q^\sigma = \left|\tilde{Q}^\sigma(k+1) - Q_{\text{ref}}^n(k)\right|, \\ &\quad g_{\text{L1}}^\sigma = \left|\tilde{I}_{\text{L1}}^\sigma(k+1) - I_{\text{L1-ref}}^n(k)\right|, \\ &\quad g_{\text{C1}}^\sigma = \left|\tilde{V}_{\text{C1}}^\sigma(k+1) - V_{\text{C1-ref}}^n(k)\right|. \end{aligned} \tag{18}$$

In this cost function, n indicates the value of weighting factors associated with each mode of operation. Since we have a hybrid MPC cost function for each mode of operation (MPPT and LVRT), the weight factors (λ'_n, λ''_n, δ'_n, δ''_n) are selected adaptively based on the modes of operations. The system operates in MPPT and LVRT modes for $n = 1$ and 2, respectively. According to (18), two sets of the weight factors coefficient are selected: one set for MPPT mode ($n = 1$) and another set for LVRT mode ($n = 2$). If there is no grid voltage sag, then $\lambda'_{n=1}$, $\lambda''_{n=1}$, $\delta'_{n=1}$, $\delta''_{n=1} \neq 0$, and if the voltage sag is detected, then $\lambda'_{n=1}, \lambda''_{n=1}, \delta'_{n=1}, \delta''_{n=1} = 0$ and $\lambda'_{n=2}, \lambda''_{n=2}, \delta'_{n=2}, \delta''_{n=2} \neq 0$. This method of the formulation will provide more flexibility to improve the dynamic performance of the reactive current injection to the grid in the LVRT mode for the provision of ancillary services. Similarly, in case of MPPT operation mode, priority can be given to PV power harvesting under dynamic PV ambient conditions.

The non-zero weights' factors are determined using the branch and bound technique [39, 40] in order to minimise the number of required simulations to find appropriate weight factors. This technique first identifies a couple of initial values for the weight factors (for example, four values), commonly with different orders to have a very wide range. Then, control objectives will be used as a measurement tool to narrow down the range of initially identified four weight factors by eliminating weight factors that does not meet the desired performance. Assuming that only two of the initially selected weight factors yield acceptable results, then four new weight factors will be chosen for further tuning. This procedure is continued to finally determine optimal weight factors. In this paper, we have chosen the tracking errors of each control objectives and injected grid current total harmonic distortion (THD) as a measurement tool for selection of weight factors using the branch and bound technique.

The I_{L1-ref} in MPPT mode is calculated from the determined maximum available PV power (P_{PV}) and the V_{PV} at MPP. In the LVRT mode, the I_{L1-ref} is calculated according to the required reactive and active powers that should be injected into the grid using the constant peak current method. In the LVRT mode, the system is not operating at its MPP, thus the P_{PV} and as a result I_{L1-ref} will shift from MPP coordinates as shown in Fig. 5. The capacitor C_1 voltage should be greater than double the grid voltage [41], thus the V_{C1-ref} is chosen to be $2.5 \times V_{grid}$. Finally, the cost function (18) is minimised based on the system model for all active, zero, and shoot-through states ($\sigma \in [1, 5]$) and the calculated references according to the mode of operation. The predictions of the values of the control variables are obtained for each feasible voltage vector state, and the cost function (18) is calculated accordingly for each of these voltage vectors. The switching state σ that minimises the cost function J^{σ} will be applied to the ZSI in Fig. 1.

3 Results and discussion

The proposed system, illustrated in Fig. 1 with parameters given in Table 1, is tested experimentally for several case studies in MPPT mode with normal grid condition and LVRT mode in case of grid voltage sag occurrence. The sampling time T_s is 60 µs; this sampling time is chosen based on the desired performance and complexity of the control scheme while considering the capability of the hardware microprocessor (dSPACE 1006 platform) we used for the system test. A programmable bidirectional ac power source by Chroma (Regenerative Grid Simulator model 61830) is used as the grid in the experiments to emulate low-voltage scenarios. The switching devices used for ZSI are C3M0075120J for Inverter Bridge and C4D15120D for the diode. The current and voltage sensors are CAS 25-NP and LV25-600, respectively; other system parameters are listed in Table 1.

Table 1 System parameters

Parameter	Value
C_1	1000 µF
C_2	1000 µF
L_1	0.7 mH
L_2	0.7 mH
sampling time	60 µs
C_{pv}	470 µF
L_{grid}	1 mH
C_{grid}	470 µF

Fig. 6 illustrates the proposed predictive model of the control objectives for MPC cost function. Figs. 6*a* and *b* show the predictive model of inductor current and capacitor voltage in the impedance network (L_1 and C_1) for shoot-through mode and non-shoot-through mode, respectively. These predicted models depend on the system model parameters and sampling time T_S. Fig. 6*c* shows the predicted active and reactive powers (P and Q) for regulating them based on MPPT and LVRT reference generations through MPC cost function (18).

The performance of the proposed system is evaluated by looking into the following important merit criteria: harvesting the maximum power with small oscillation around MPP, fast dynamic response under dynamic PV ambient condition, robust operation under grid voltage sag, reactive power injection support in LVRT mode according to grid standards and codes such as E.ON standard [32], decoupled active and reactive power controls in the MPPT mode without affecting the boosting operation of ZSI, and high-quality current injection to the grid considering the THD limits according to IEEE-519 standards [7].

To start the experiments, the system is initially tested in normal grid condition with the objective to operate at MPPT with unity power factor. The resulting waveforms for this condition are shown in the scope shot of Fig. 7*a*. Remaining in the healthy grid condition, the system is tested through a more realistic scenario in which the grid voltage has distortions. In this experiment, the highest allowed values of 3rd, 5th, 7th, and 11th-order harmonics according to IEEE-519 standards [7] are added to grid voltage (v_g) using a programmable ac power source. As shown in the scope shot of Fig. 7*b*, the control objectives are achieved perfectly even in the presence of grid voltage harmonics.

The performance of the controller during a grid voltage sag event (due to a fault) is tested next. The resulting waveforms are shown in the scope shots of Figs. 7*c* and *d*. In this experiment, the system is initially operating with normal grid condition at unity power factor. Subsequently, at time instant t_1, the sag detector detects 25% voltage sag in the grid voltage and according to the LVRT operation requirement and depth of sag, the ZSI is triggered to inject 400 VAR reactive power into the grid. As pictured in Fig. 7*c*, the peak of the grid current is kept constant before and after the reactive current injection, thus achieving the proposed predictive controller objective to maintain constant peak current in this mode of operation. Later, at instant t_2 the grid voltage returns to normal condition, and the controller is triggered to return to MPPT operation mode at unity power factor as shown in Fig. 7*d*. This experiment verifies the MPC-enabled LVRT capability of ZSI and seamless transition between MPPT and LVRT modes for the proposed dual-mode grid-tied ZSI.

The last experiment is examining the response of the system to a change in solar irradiance in normal and faulty grid conditions. The effect of solar irradiance changes in normal grid condition (MPPT mode) is illustrated in Fig. 8*a*. The solar irradiance is initially at 1000 W/m^2, then at time t_3 the solar irradiance is stepped down to 700 W/m^2. As pictured, the peak grid current and inductor L_1 current are decreased according to the P–V characteristic of the PV panel. The grid current is maintained constant according to the available power from the PV panel and the step change in solar irradiance did not cause any inrush grid current. Fig. 8*b* illustrates the response of the proposed system to step change in solar irradiance after the sag detector detects a 25% grid voltage sag and puts the system in the LVRT mode. The solar irradiance is initially at 700 W/m^2, then at time t_4 the solar irradiance is stepped up to 1000 W/m^2. As pictured, this change causes an increase in the grid peak current and inductor L_1 current. This case study demonstrates the capability of adjusting the power drawn from the PV panel by moving along the P–V characteristic curve of PV panel according to available solar irradiance and depths of voltage sag to maintain LVRT operation requirement.

Finally, the active and reactive powers for experiments in Figs. 7*c* and *d* are obtained from an oscilloscope and plotted in MATLAB for better observation of dynamic response of the controller when the sag detector detects 25% grid voltage sag. As it

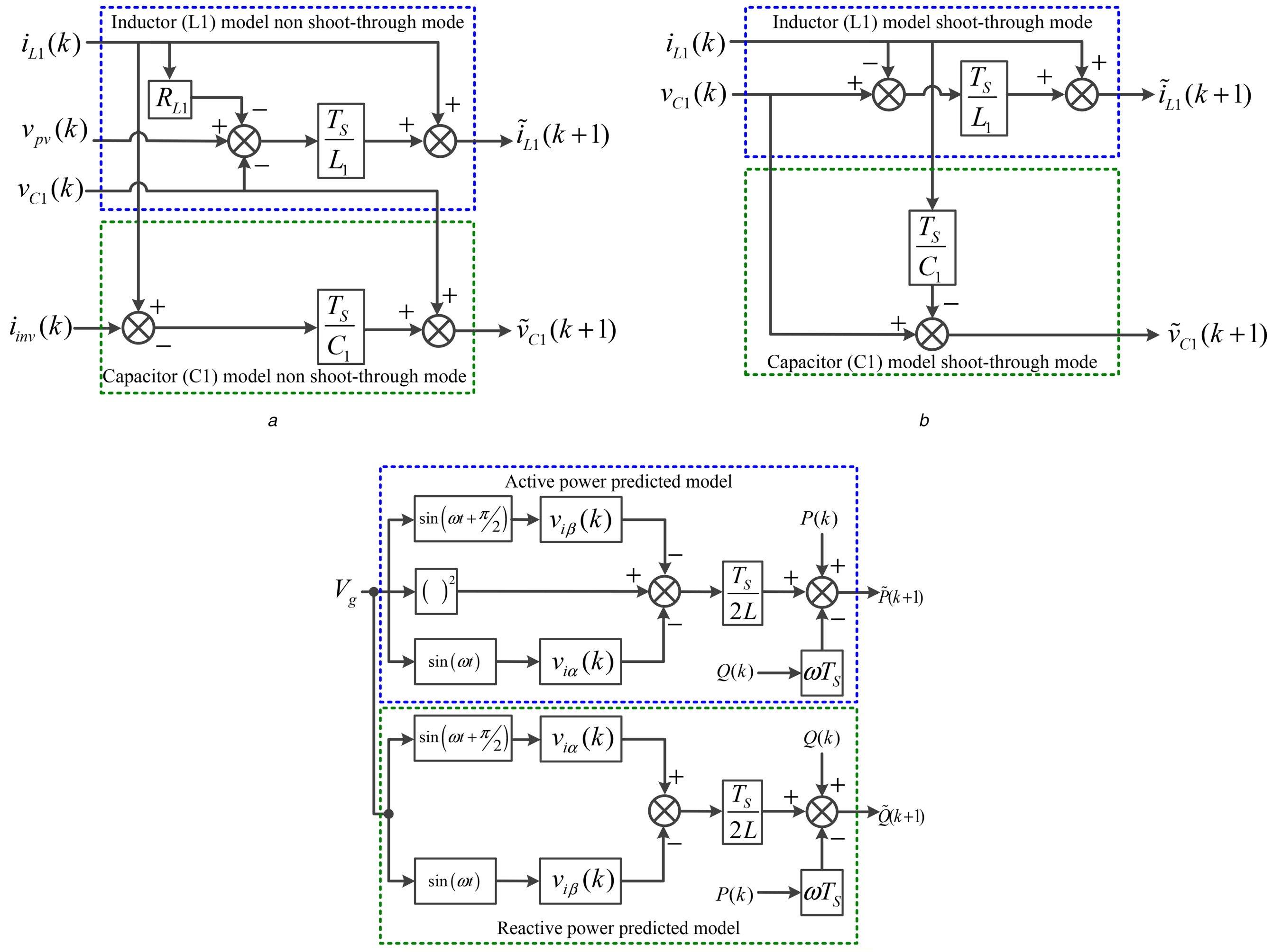

c

Fig. 6 *Proposed MPC block diagram*
(a) Predictive model of the inductor current and capacitor voltage (L_1, C_1) in non-shoot-through mode, ***(b)*** Predictive model of the inductor current and capacitor voltage in shoot-through mode, ***(c)*** Active and reactive power predictive models

is shown in Fig. 9, the level of active power injected into the grid is decreased to provide sufficient room for reactive power injection according to LVRT control mode requirement. Owing to the capability of MPC for predicting the error before applying the switching state to the ZSI, the change in the mode of operation from MPPT to LVRT and vice versa is achieved seamlessly. As it is shown in Fig. 9, the proposed predictive controller for ZSI, without the requirement of challenging tuning in each mode of operation, has a promising dynamic response and high control efficacy in steady-state operation. Similarly, as pictured in the scope shots of Fig. 8, the proposed predictive controller effectively shifts the operating point of the ZSI along the *P–V* characteristic curve of the PV panel to maximise the energy harvest and provide the required reactive power without inrush grid current or diminishing the grid power quality. The individual harmonic components of the grid-side current, i_g, are presented in Table 2. The calculated THD of i_g is 2.87% which is within the IEEE-519 standards for grid-tied systems.

One of the main drawbacks of the MPC is the effect of model parameters mismatch (error) on the controller performance. As an additional performance analysis of the proposed control strategy, Fig. 10 shows the effects of the variations of L_1 and L from their nominal values (model parameter mismatch) on MPP tracking accuracy and grid-side current THD. In this figure, the robustness of the proposed control scheme is analysed from −40 to +80% error in the L_1 and L models, where 0% error demonstrates no model parameter mismatch. Fig. 10*a* shows the effect of the grid-side filter inductance model mismatch on injected current THD. As it is shown for most of the scenarios, the variations of THD values are not much and they are within the IEEE-519 standards and around 2.8% at standard test condition (0% model parameter mismatch). Furthermore, Fig. 10*b* shows that the variation of the expected MPP from the measured harvested PV power is <5 W which is negligible.

4 Conclusion

This paper proposes a single-stage PEI based on impedance-source inverter for PV applications with LVRT capability during the grid voltage sag according to grid standards. By using the MPC framework, a simple control strategy is proposed with an adaptive cost function to seamlessly operate under normal and faulty grid conditions. The proposed system eliminates the requirements of multi–nested-loop of classical controller. Owing to the predictive nature of the controller, the proposed system has fast dynamic response to change in solar irradiance or grid reactive power requirement according to LVRT operation. The system is switching between LVRT and MPPT modes of operations seamlessly. The proposed system can be extended for overnight operation of PV sources in DGs with reactive power compensation capability as ancillary service from DG to main grid. Several experiments have been conducted to verify the performance of the proposed system. The results demonstrate robust operation, MPP operation during the healthy grid condition, high-power quality injection during steady-state condition, negligible overshoot/undershoot in grid current injection due to change in solar irradiance or reactive power reference, no observation of inrush current during dynamic change in MPC cost function references for LVRT operation, and maintaining constant peak grid current during the LVRT mode.

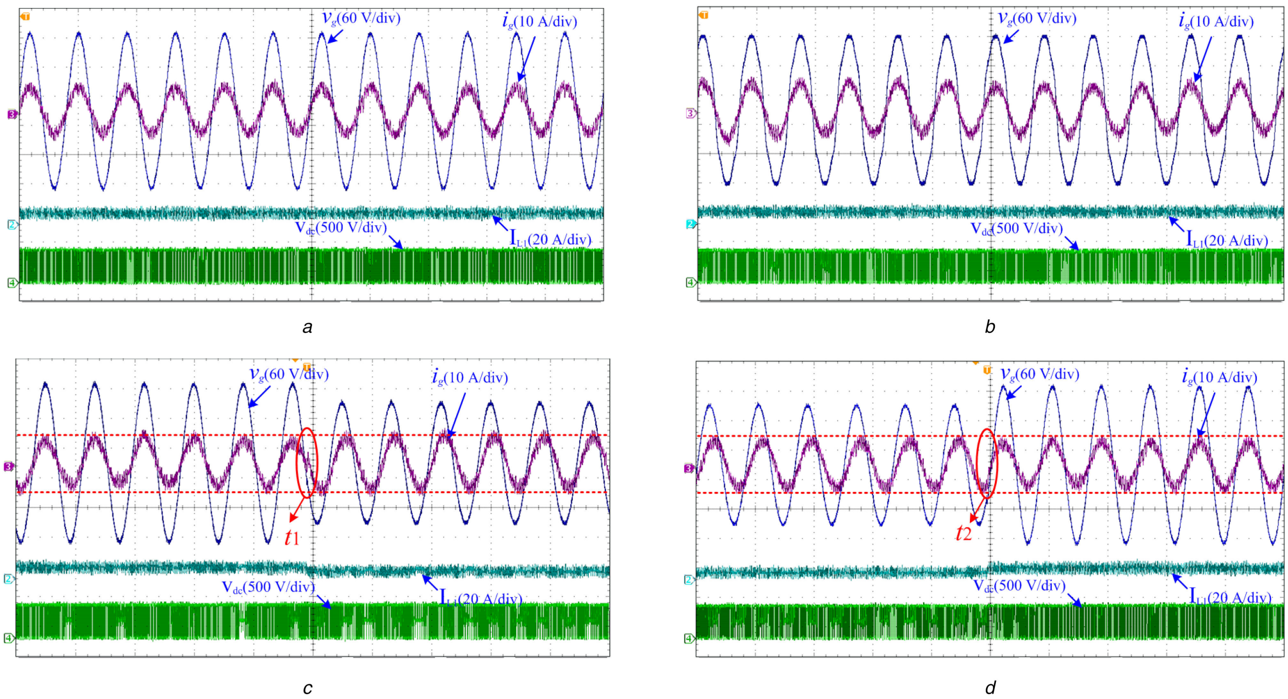

Fig. 7 *System performance evaluation in steady-state MPPT mode and transition between LVRT and MPPT modes*
(a) Grid voltage (v_g), grid current (i_g), inductor L_1 current (I_{L1}), and pulsating dc-link voltage (V_{dc}) when the system is operating in MPPT mode and unit power factor in normal grid condition, ***(b)*** Grid voltage (v_g), grid current (i_g), inductor L_1 current (I_{L1}), and pulsating dc-link voltage (V_{dc}) when the system is operating in MPPT mode and unit power factor in normal grid condition with distorted grid voltage, ***(c)*** Grid voltage (v_g), grid current (i_g), inductor L_1 current (I_{L1}), and pulsating dc-link voltage (V_{dc}) when the 25% grid voltage sag occurs at t_1 and the system changes its mode of operation from MPPT to LVRT with reactive current injection, ***(d)*** Grid voltage (v_g), grid current (i_g), inductor L_1 current (I_{L1}), and pulsating dc-link voltage (V_{dc}) when the grid goes back to normal condition at t_2 and the system changes its mode from LVRT to MPPT with unity power factor

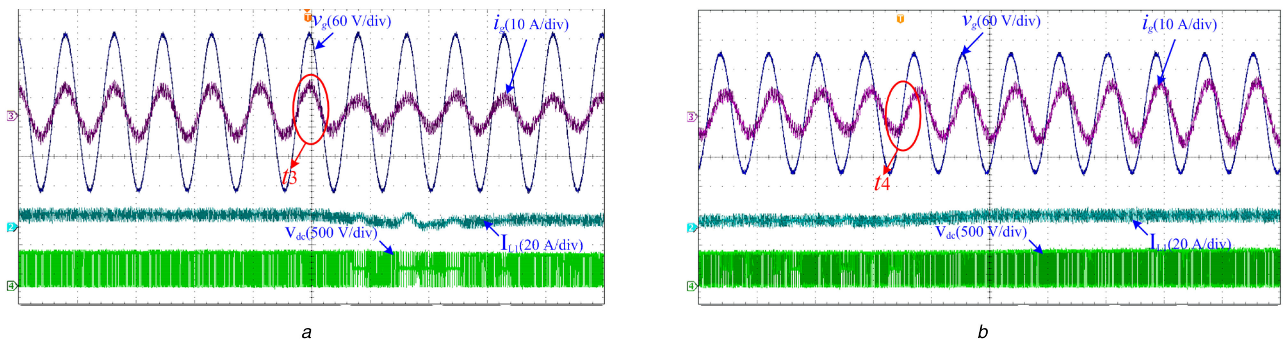

Fig. 8 *System performance evaluation to changes in solar irradiance in MPPT and LVRT modes*
(a) Grid voltage (v_g), grid current (i_g), inductor L_1 current (I_{L1}), and pulsating dc-link voltage (V_{dc}) with a step change in solar irradiance level from 1000 to 700 W/m^2 at time t_3 when the system is operating in MPPT mode under normal grid condition, ***(b)*** Grid voltage (v_g), grid current (i_g), inductor L_1 current (I_{L1}), and pulsating dc-link voltage (V_{dc}) with step change in solar irradiance level from 700 to 1000 W/m^2 at time t_4 when the system is operating in LVRT mode and 25% grid voltage sag

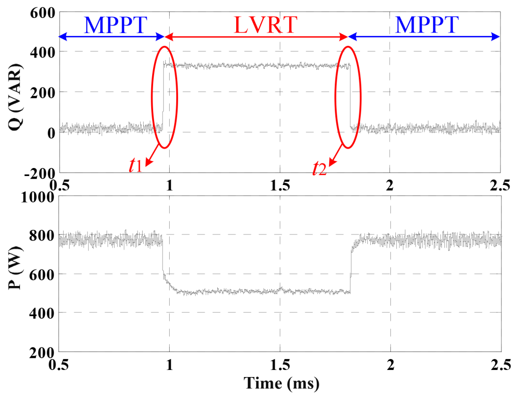

Fig. 9 *Active and reactive powers when the grid voltage sag of 25% occurs for time intervals t_1–t_2. The system is operating in normal grid condition before t_1 and after t_2*

Table 2 Grid current harmonic distortions

Harmonics order	Distortion, %
3rd	0.79
5th	1.1
7th	0.34
9th	0.28
11th	0.18
13th	0.06
15th	0.04
17th	0.08

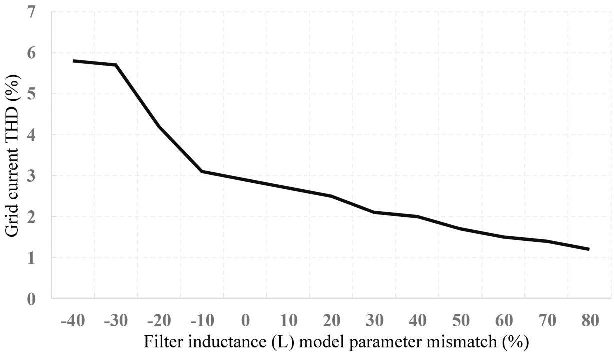

a

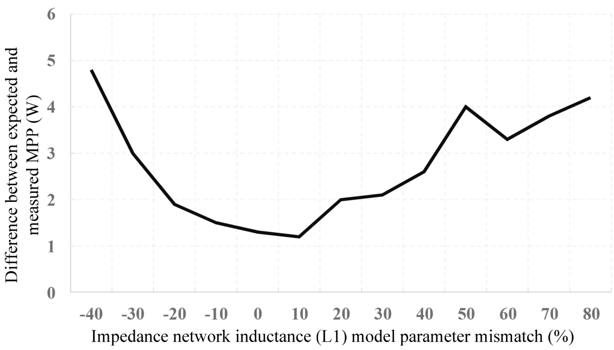

b

Fig. 10 *Effect of model parameter mismatch on the proposed control scheme*

(a) Effect of grid-side filter inductance (L) model parameter mismatch (%) on grid current quality (THD), ***(b)*** Effect of impedance network inductance (L_1) model parameter mismatch (%) on MPP tracking accuracy

5 References

[1] Cho, Y.W., Cha, W.J., Kwon, J.M.*, et al.*: 'Improved single-phase transformerless inverter with high power density and high efficiency for grid-connected photovoltaic systems', *IET Renew. Power Gener.*, 2016, **10**, pp. 166–174

[2] Guo, X.Q., Wu, W.Y.: 'Improved current regulation of three-phase grid-connected voltage-source inverters for distributed generation systems', *IET Renew. Power Gener.*, 2010, **4**, pp. 101–115

[3] Hosseinzadeh, M., Salmasi, F.R.: 'Power management of an isolated hybrid AC/DC micro-grid with fuzzy control of battery banks', *IET Renew. Power Gener.*, 2015, **9**, pp. 484–493

[4] Shadmand, M.B., Mosa, M., Balog, R.S.*, et al.*: 'Model predictive control of a capacitorless matrix converter-based STATCOM', *IEEE J. Emerg. Sel. Top. Power Electron.*, 2017, **5**, pp. 796–808

[5] Momeneh, A., Castilla, M., Miret, J.*, et al.*: 'Comparative study of reactive power control methods for photovoltaic inverters in low-voltage grids', *IET Renew. Power Gener.*, 2016, **10**, pp. 310–318

[6] Chilipi, R., Al Sayari, N., Al Hosani, K.*, et al.*: 'Control scheme for grid-tied distributed generation inverter under unbalanced and distorted utility conditions with power quality ancillary services', *IET Renew. Power Gener.*, 2016, **10**, pp. 140–149

[7] I.W. Group: 'IEEE recommended practices and requirements for harmonic control in electrical power systems', IEEE STD, 1992, pp. 519–1992

[8] 'IEEE standard for interconnecting distributed resources with electric power systems', IEEE Std. 1547-2003, 2003, pp. 1–28

[9] I.E. Commission: 'Characteristics of the utility interface for photovoltaic (PV) systems'. Report of IEC, 2002, vol. 61727

[10] 'IEEE guide for monitoring, information exchange, and control of distributed resources interconnected with electric power systems', IEEE Std. 1547.3-2007, 2007, pp. 1–160

[11] Marafão, F.P., Brandão, D.I., Costabeber, A.*, et al.*: 'Multi-task control strategy for grid-tied inverters based on conservative power theory', *IET Renew. Power Gener.*, 2014, **9**, pp. 154–165

[12] Jou, H.-L., Chiang, W.-J., Wu, J.-C.: 'Virtual inductor-based islanding detection method for grid-connected power inverter of distributed power generation system', *IET Renew. Power Gener.*, 2007, **1**, pp. 175–181

[13] Bei, T.-Z.: 'Accurate active islanding detection method for grid-tied inverters in distributed generation', *IET Renew. Power Gener.*, 2017, **11**, pp. 1633–1639

[14] Yang, Y., Blaabjerg, F., Wang, H.: 'Low-voltage ride-through of single-phase transformerless photovoltaic inverters', *IEEE Trans. Ind. Appl.*, 2014, **50**, pp. 1942–1952

[15] Tang, C.Y., Chen, Y.T., Chen, Y.M.: 'PV power system with multi-mode operation and low-voltage ride-through capability', *IEEE Trans. Ind. Electron.*, 2015, **62**, pp. 7524–7533

[16] Yang, Y., Blaabjerg, F., Wang, H.*, et al.*: 'Power control flexibilities for grid-connected multi-functional photovoltaic inverters', *IET Renew. Power Gener.*, 2016, **10**, pp. 504–513

[17] Kjaer, S.B., Pedersen, J.K., Blaabjerg, F.: 'A review of single-phase grid-connected inverters for photovoltaic modules', *IEEE Trans. Ind. Appl.*, 2005, **41**, pp. 1292–1306

[18] Kouro, S., Leon, J.I., Vinnikov, D.*, et al.*: 'Grid-connected photovoltaic systems: an overview of recent research and emerging PV converter technology', *IEEE Ind. Electron. Mag.*, 2015, **9**, pp. 47–61

[19] Shao, Z., Zhang, X., Wang, F.*, et al.*: 'Analysis and control of neutral-point voltage for transformerless three-level PV inverter in LVRT operation', *IEEE Trans. Power Electron.*, 2017, **32**, pp. 2347–2359

[20] Fang Zheng, P.: '*Z*-source inverter', *IEEE Trans. Ind. Appl.*, 2003, **39**, pp. 504–510

[21] Tang, Y., Wei, J., Xie, S.: 'Grid-tied photovoltaic system with series *Z*-source inverter', *IET Renew. Power Gener.*, 2013, **7**, pp. 275–283

[22] Sun, D., Ge, B., Yan, X.*, et al.*: 'Modeling, impedance design, and efficiency analysis of quasi-*Z*-source module in cascaded multilevel photovoltaic power system', *IEEE Trans. Ind. Electron.*, 2014, **61**, pp. 6108–6117

[23] Zhang, J.: 'Unified control of *Z*-source grid-connected photovoltaic system with reactive power compensation and harmonics restraint: design and application', *IET Renew. Power Gener.*, 2018, **12**, (4), pp. 422–429

[24] Singh, S.A., Carli, G., Azeez, N.A.*, et al.*: 'Modeling, design, control, and implementation of a modified *Z*-source integrated PV/grid/EV DC charger/inverter', *IEEE Trans. Ind. Electron.*, 2018, **65**, pp. 5213–5220

[25] Shen, H., Zhang, B., Qiu, D.: 'Hybrid *Z*-source boost DC–DC converters', *IEEE Trans. Ind. Electron.*, 2017, **64**, pp. 310–319

[26] Rodriguez, J., Kazmierkowski, M.P., Espinoza, J.R., :*, et al.*: 'State of the art of finite control set model predictive control in power electronics', *IEEE Trans. Ind. Inf.*, 2013, **9**, pp. 1003–1016

[27] Mosa, M., Shadmand, M.B., Balog, R.S.*, et al.*: 'Efficient maximum power point tracking using model predictive control for photovoltaic systems under dynamic weather condition', *IET Renew. Power Gener.*, 2017, **11**, pp. 1401–1409

[28] Bayhan, S., Trabelsi, M., Abu-Rub, H.*, et al.*: 'Finite-control-set model-predictive control for a quasi-*Z*-source four-leg inverter under unbalanced load condition', *IEEE Trans. Ind. Electron.*, 2017, **64**, pp. 2560–2569

[29] Abu-Rub, H., Liu, Y., Ge, B.*, et al.*: '*Impedance source power electronic converters*' (Wiley-IEEE Press, 2016)

[30] Xiao, F., Dong, L., Li, L.*, et al.*: 'A frequency-fixed SOGI-based PLL for single-phase grid-connected converters', *IEEE Trans. Power Electron.*, 2017, **32**, pp. 1713–1719

[31] Akagi, H., Watanabe, E.H., Aredes, M.: '*Instantaneous power theory and applications to power conditioning*', vol. **62**, (Wiley-IEEE Press, 2016)

[32] Netz, E.: '*Grid code; high and extra high voltage*', vol. **4**, (E-One Netz GmbH, Bayreuth, 2006)

[33] Carrasco, J.E.-G., Tena, J., Ugena, D.*, et al.*: 'Testing low voltage ride through capabilities of solar inverters', *Electr. Power Syst. Res.*, 2013, **96**, pp. 111–118

[34] Neumann, T., Erlich, I.: 'Modelling and control of photovoltaic inverter systems with respect to German grid code requirements'. IEEE Power and Energy Society General Meeting, San Diego, CA, 2012

[35] Kovanen, K.O.: 'Photovoltaics and power distribution', *Renew. Energy Focus*, 2013, **14**, pp. 20–21

[36] Lee, C.T., Hsu, C.W., Cheng, P.T.: 'A low-voltage ride-through technique for grid-connected converters of distributed energy resources', *IEEE Trans. Ind. Appl.*, 2011, **47**, pp. 1821–1832

[37] Sajadian, S., Ahmadi, R.: 'Model predictive based maximum power point tracking for grid-tied photovoltaic applications using a *Z*-source inverter', *IEEE Trans. Power Electron.*, 2016, **31**, pp. 7611–7620

[38] Sangwongwanich, A., Yang, Y., Blaabjerg, F.: 'High-performance constant power generation in grid-connected PV systems', *IEEE Trans. Power Electron.*, 2016, **31**, pp. 1822–1825

[39] Cortes, P., Kouro, S., La Rocca, B.*, et al.*: 'Guidelines for weighting factors design in model predictive control of power converters and drives'. IEEE Int. Conf. Industrial Technology, Gippsland, 2009

[40] Rodriguez, J., Cortes, P.: '*Predictive control of power converters and electrical drives*', vol. **40**, (Wiley-IEEE Press, 2012)

[41] Li, Y., Jiang, S., Cintron-Rivera, J.G.*, et al.*: 'Modeling and control of quasi-*Z*-source inverter for distributed generation applications', *IEEE Trans. Ind. Electron.*, 2013, **60**, pp. 1532–1541